Modeling Low-Temperature–Induced Failure of Pressurized Pipelines

Haroun Mahgerefteh and Olufemi Atti
Dept. of Chemical Engineering, University College London, London WC1E 7JE, United Kingdom

DOI 10.1002/aic.10719
Published online October 28, 2005 in Wiley InterScience (www.interscience.wiley.com).

The development of a rigorous mathematical model for simulating the processes leading to the transition of an initially stable through-wall defect into an elongated running fracture in pressurized pipelines is described. The application of the model to the puncture of a gas pipeline followed by its isolation indicates significant and rapid localized cooling of the pipe wall to temperatures well below its ductile to brittle transition temperature. The resulting order of magnitude drop in the fracture toughness coupled with the pressure stresses at the defect plane are shown to lead to catastrophic pipeline failure in the form of a running fracture some 2000 s after its puncture. Significantly, delay in pipeline isolation after its puncture is shown to have a profound effect in circumventing such failures. The above study for the first time quantitatively highlights the importance of taking into account the expansion-induced cooling effects as a credible failure scenario when undertaking safety assessment of pressurized pipelines.
 AIChE J, 52: 1248–1256, 2006
Keywords: risk assessment, safety, modeling, depressurization, stress-induced failure

Introduction

Large amounts of flammable pressurized hydrocarbons are frequently transported in pipelines across the globe, passing through both rural and populated areas. Although pipelines are considered as the safest mode of transportation, accidents involving pipeline rupture do occur and the consequences can be catastrophic. During the *Piper Alpha* tragedy, for example (Cullen, 1990), the heat intensity after the rupture and ignition of the main gas export pipeline resulted in the eventual collapse of the platform into the seabed, the loss of 167 lives, and a cost of £2 billion. The impact on the environment after pipeline failure can also be equally devastating. More than 6.3 million gallons of oil and other hazardous liquids, on average, are reported released from pipelines each year, more than half the amount released from the *Exxon Valdez* disaster (Environmental Defence, 1999). In the United States, record negligence fines are being imposed on operators whose pipelines rupture and cause casualties or damage to the environment (Barlas, 1999).

During the course of a series of recent studies (Mahgerefteh et al., 1997, 1999, 2000; Oke et al., 2003), we developed a robust numerical simulation based on the method of characteristics (Zucrow, 1976) for simulating outflow after pipeline rupture. The model accounts for all of the important processes taking place during depressurization, including real fluid behavior, frictional effects, radial and axial flow in the proximity of a puncture, and the accompanying rapid pressure and thermal oscillations. Orders of magnitude reduction in computer run times have been achieved through the development of this fast numerical simulation technique. Very good agreement between simulation results with field data was obtained.

An important observation made during our investigations and also confirmed by others (Saville et al., 2004) was that in the case of stable, through-wall defects or punctures in pressurized pipelines containing certain low molecular weight hydrocarbons such as methane or ethylene, the rapid quasi-adiabatic depressurization results in significant cooling of the escaping fluid to temperatures as low as −100°C. In the case of buried pipelines, where there is no blowout of material, the

Correspondence concerning this article should be addressed to H. Mahgerefteh at h.mahgerefteh@ucl.ac.uk.

escaping fluid will gradually chill down the surrounding soil, freezing any moisture. This will in turn envelop a section of the pipeline with a cold insulating blanket. If the pipe wall temperature reaches its ductile/brittle transition temperature (typically −20 to −70°C), a rapid marked decrease in the pipeline's fracture toughness will occur (Rinebolt and Harris, 1951). Under such circumstances it is imperative to be able to predict a priori whether the corresponding thermal and pressure stresses at the crack tip would lead to its transformation into a propagating fracture. In such a case, the ignition of the massive amount of escaped inventory will in turn result in an enormous vapor cloud explosion, causing significant damage and fatalities in populated areas.

Indeed in recent months, there have been three major incidents: Alberta, Canada, December 2 and 3, 2003 (http://www.transcanada.com/news/2003_news/2003_12_04.html); Brussels, Belgium, July 30, 2004 (http://news.bbc.co.uk/1/hi/world/europe/3939087.stm), where an initial leak from the buried gas pipelines was followed by rupture and massive explosions a few minutes later. The Belgium incident resulted in 24 deaths and 120 injuries.

The problem of low-temperature–induced fracture propagation has become even more pressing in view of the fact that to meet the rapid global increase in demand for gas while reducing capital costs, new high-strength steel long-distance pipelines capable of operating at higher pressures are being considered. An important consideration governing the introduction of these steels is the ability to demonstrate that propagating fractures will not occur, or to show that arrest will occur within a small length of the pipeline. Central to addressing the above is the ability to accurately predict the discharge pressure at the crack, the accompanying transient local temperature and pressures stresses, and their variation with time using a real fluid model.

Surprisingly, despite the fact that low-temperature–induced brittle fracture during the rapid depressurization or blowdown of pressurized vessels has received considerable attention (see, for example, Haque et al., 1992a; Mahgerefteh and Wong, 1999), little work of the similar nature has been reported in the case of pressurized pipelines. This is remarkable considering that running fractures in pipelines were first reported as early as 1950s with a number of these failures propagating for several kilometers before arresting at a valve location or thicker pipe wall (Horsley, 2003).

Maxey et al. (1974, 1975) developed a model based on coupling the fluid decompression trajectory accounting for two-phase flow with an empirically calibrated correlation for fracture behavior. Ives et al. (1974) reported that the primary driving force for ductile fracture propagation in pipelines containing high-pressure gases is the residual pressure of the escaping fluid acting on the wall interior downstream of the crack. Picard and Bishnoi (1988) highlighted the importance of accounting for real fluid behavior and nonisentropic effects such as heat transfer and friction for predicting the correct fluid discharge pressure in fracture propagation analysis.

Despite its obvious importance, none of the above studies fully accounts for the role of fluid/structure interactions including the pertinent thermodynamic, heat transfer, and real fluid effects on the fracture propagation process in pressurized pipelines. In addition, fracture mechanics analyses of this subject area are generally empirically based (API, 2000), meaning that the understanding gained and results are not easily extrapolated to situations where operating parameters are different. Hydrotesting of pipelines (Duffy, 1969) before commissioning can induce warm prestressing, which has been shown to some extent to reduce the pipeline's susceptibility to low-temperature–induced brittle fracture. Once again though, no systematic fundamental studies identifying the governing mechanism and quantifying the effectiveness of the warm prestressing have yet been undertaken. As such, there is no certainty whether and how warm prestressing will reduce the risk of low-temperature–induced fracture propagation in newly introduced high-strength pipelines. To optimize operating parameters and to develop crack arrest philosophies, an integrated analytical approach is necessary.

We describe herein the development of a rigorous mathematical model for simulating low-temperature–induced fracture propagation in pressurized pipelines. The model is tested based on a hypothetical case example involving a through-wall defect in a carbon steel pressurized pipeline containing a multicomponent hydrocarbon mixture. Two types of failure scenarios involving isolated and nonisolated release where pumping continues despite pipeline puncture are simulated. This is followed by a pictorial timeline simulation of the sequence of events commencing with the fluid discharge, the propagation of a cold-temperature front along the defect plane (parallel to the major pipeline axis), the defect growth, and its critical transition into an unstable fracture culminating in catastrophic pipeline failure.

Theory

The physical problem under consideration is the sequence of events after the formation of a stable through-wall defect or puncture in a pipeline containing a condensable gas mixture at high pressure. Loss of gas causes depressurization at the rupture plane, and a wave of low pressure will travel away from the rupture site, typically starting as an expansion fan. Within this fan, the gas may condense, forming a two-phase flow. We sought to determine the conditions of flow within the pipe, the exiting fluid properties, and the accompanying fluid/structure interactions manifested in the localized thermal and pressure stresses in the pipe wall. This task requires the modeling of the following interacting processes:

(1) Fluid dynamics such as the discharge rate, fluid temperature, and fluid pressure at the defect plane using a real fluid model

(2) Heat transfer effects between the escaping fluid, pipe wall, and the surrounding ambient

(3) Pressure and thermal stresses within the defect plane

(4) Fracture propagation

Fluid dynamics

The governing theory for determining the fluid dynamics such as the discharge rate and the fluid, temperature, pressure, and velocity profiles along the pipeline after its puncture has been described in our earlier publication (Oke et al., 2003) and thus only a brief account of the main features is given here. The procedure in essence involves the numerical solution of the mass, energy, and momentum conservation equations using a suitable technique such as the method of characteristics (MOC;

Zucrow, 1976). The model, validated against field data, accounts for real fluid behavior, heat transfer, and frictional effects as well as radial and axial flow near the rupture plane. It is applicable to both isolated and nonisolated flows where pumping at the high-pressure end continues despite puncture.

Liquid and vapor phases are assumed to be at thermodynamic and phase equilibrium with one another traveling at the same velocity. This assumption is found to be generally valid in the case of rupture of long pipelines (Saha, 1997). In the case of short pipelines (<100 m) such as the cooling tubes used in pressurized water reactors, a heterogeneous equilibrium model may be more appropriate. The model proposed by Markatos et al. (1983, 1984), for example, accounts for phase slip. However, the simulation has been applied only to water/steam mixtures using correlations that are not available for the more complex multicomponent hydrocarbon systems. On the other hand, application of the water/steam heterogeneous equilibrium model of Philbin (1991) to hydrocarbons produces very poor agreement with real data (Mahgerefteh et al., 1999).

The fluid approaching the puncture during depressurization can be either single phase or two phase. If the backpressure is sufficiently low, the fluid accelerates through the orifice at its maximum velocity and expands rapidly from the upstream to the orifice pressure. Consequently, condensation may occur, which results in two-phase flow. The procedure for determination of the discharge rate and the state of fluid phase at the orifice is described elsewhere (Haque et al., 1992a; Mahgerefteh and Wong, 1999). In essence, it is based on carrying out an energy balance across the orifice assuming isentropic expansion coupled with thermodynamic and phase equilibrium.

The flow-dependent wall friction force term is obtained using the Moody approximation (Massey, 1983) to the Colebrooke equation.

The Peng–Robinson equation of state (EoS; Peng and Robinson, 1976) is used to obtain the appropriate thermodynamic and phase equilibrium data. This equation has been shown to be particularly applicable to high-pressure hydrocarbon mixtures (see, for example, Assael et al., 1996; de Reuck et al., 1996). The number and the appropriate fluid phase(s) present at any given temperature and pressure on the other hand are determined using the stability test based on the Gibbs tangent plane criterion developed by Michelsen (1982a,b, 1987). For unstable systems, the same technique also provides the composition of a new phase, which can be split off to decrease the Gibbs energy of the mixture. Pseudo-fluid properties for mixtures are calculated from the pure liquid and gas properties obtained from the EoS.

The speed of sound for real multicomponent single-phase fluids is obtained using standard expressions (see, for example, Picard and Bishnoi, 1987). In the absence of an analytical solution, the speed of sound for two-phase mixtures is calculated numerically (Mahgerefteh et al., 2001).

Heat transfer

The radial, axial, and tangential temperature profiles in the pipe wall in the proximity of a puncture are governed by the following modes of heat transfer as depicted in Figure 1:

(1) Conductive heat transfer within the pipe wall (H_1)

(2) Natural/forced convective heat transfer between the outside ambient and the pipe wall (H_2)

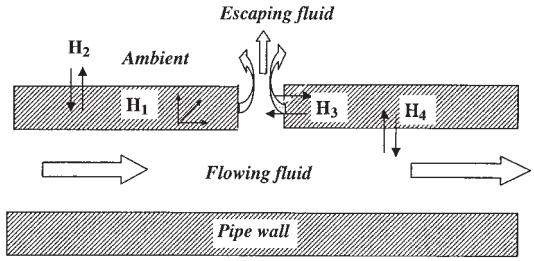

Figure 1. Various heat transfer boundaries after pipeline puncture.

(3) Axial forced convective heat transfer between the escaping fluid and the puncture plane (H_3)

(4) Forced convective heat transfer between the flowing fluid and the pipe wall (H_4)

Heat Transfer within the Pipe Wall: H_1. The radial (r), tangential (ϕ), and axial (z) temperature profiles within the pipe wall arising from conductive heat transfer are determined from the numerical solution of the heat transfer equation given by Osizik (1980):

$$\frac{\partial^2 T}{\partial r^2} + \frac{1}{r}\frac{\partial T}{\partial r} + \frac{1}{r^2}\frac{\partial^2 T}{\partial \phi^2} + \frac{\partial^2 T}{\partial z^2} = \frac{1}{\alpha}\frac{\partial T}{\partial \tau} \tag{1}$$

where T is the temperature at any point within the pipeline with α and τ, respectively, denoting thermal diffusivity and time.

In this study, the pipeline wall is divided into nodal points with the conduction equation solved numerically at each node to obtain its temperature at the next time step. The explicit finite-difference scheme (Holman, 1986) is used to resolve the equation. The time step is chosen in accordance with the stability requirement (Holman, 1986), such that

$$\mathrm{Fo}_{\min} \le \frac{1}{6} \qquad \text{and} \qquad \mathrm{Fo}_{\min}(3 + \mathrm{Bi}_{\min}) \le \frac{1}{2}$$

where $\mathrm{Fo}_{\min}$ and $\mathrm{Bi}_{\min}$ are the minimum Fourier and Biot numbers, respectively.

For the convection boundary, a transient energy balance is applied for each node so that the sum of the energies conducted and convected into the node is equal to the increase in the internal energy of the node. This requires the computation of the various phase-dependent fluid-pipeline heat transfer coefficients (see later discussion).

Fluid/Pipeline Wall Heat Transfer: H_3/H_4. In this study it is assumed that the flow after pipeline failure is fully developed and turbulent. This is a reasonable assumption, considering the relatively high Reynolds numbers ($>10^7$) after puncture. As a result, heat exchange between the flowing fluid and the pipe wall is primarily attributed to forced, as opposed to natural, convection.

For single-phase fully developed flow in smooth pipes, the correlation proposed by Gnielinski (1976), used to calculate the fluid/wall heat transfer coefficient because of its wide range of applicability and accuracy (Rohsenow et al., 1998), is given by

$$\mathrm{Nu} = \frac{(\mathrm{Re} - 1000)\mathrm{Pr}(f/2)}{1 + 12.7(f/2)^{0.5}[\mathrm{Pr}^{2/3} - 1]} \tag{2}$$

where Nu, Pr, and Re are the Nusselt, Prandtl, and Reynolds numbers, respectively:

The fanning friction factor f, in Eq. 2, is calculated from the expression proposed by Techo et al. (1965), as given by

$$\frac{1}{\sqrt{f}} = 1.7372 \ln \frac{\mathrm{Re}}{1.964 \ln \mathrm{Re} - 3.8215} \tag{3}$$

In the case of two-phase flows, the correlation proposed by Steiner and Taborek (1992) is used to calculate the heat transfer coefficient (h_f) within the pipeline. Apart from its relative simplicity and ease of use, the correlation has been shown (Rohsenow et al., 1998) to produce good agreement with experimental data for a wide range of flow regimes and is given by

$$\frac{h_f}{h_l} = \left[(1 - x)^{1.5} + 1.9x^{0.6}\left(\frac{\rho_l}{\rho_g}\right)^{0.35} \right]^{1.1} \tag{4}$$

where x is the fluid mass fraction; ρ_g and ρ_l are the vapor and liquid densities, respectively; and h_l is the heat transfer coefficient for the liquid phase, in turn given by

$$\frac{h_l D_{in}}{\kappa_l} = 0.023\left[\frac{\rho_{mix} u(1 - x) D_{in}}{\mu_l}\right]^{0.8}\left[\frac{\mu_l C_{pl}}{\kappa_l}\right]^{0.4} \tag{5}$$

The two-phase mixture density ρ_{mix} is given by

$$\rho_{mix} = \frac{\rho_g \rho_l}{\rho_g(1 - x) + \rho_l x} \tag{6}$$

Gas and liquid viscosities required for the above calculations are obtained according to Ely and Hanley (gaseous mixtures) and Dymond and Assael (liquid mixtures) schemes (Massey, 1983).

Ambient/Pipeline Wall Heat Transfer: H_2. The heat transfer coefficient h_{amb}, between the pipe wall and the surrounding ambient, is given by (Incropera and DeWitt, 1996; Rohsenow et al., 1998)

$$h_{amb} = (h_{nat}^3 + h_{for}^3)^{1/3} \tag{7}$$

where h_{nat} and h_{for} are the natural and forced heat transfer coefficients, respectively.

For natural convection, the correlation proposed by Churchill and Chu (1975) is used:

$$\frac{h_{nat} D_{out}}{\kappa_{film}} = \left[0.60 + \frac{0.387\ \mathrm{Ra}_D^{1/6}}{[1 + (0.559/\mathrm{Pr}_{film})^{9/16}]^{8/27}} \right]^2 \tag{8}$$

The dimensionless groups are defined as

$$\mathrm{Ra}_D = \mathrm{Gr}_{film}\mathrm{Pr}_{film} \qquad \text{(Rayleigh number)} \tag{9}$$

$$\mathrm{Gr}_{film} = \frac{\rho_{film}^2 g \xi_{film}(T_s - T_{amb}) D_{out}^3}{\mu_{film}^2} \qquad \text{(Grashof's number)} \tag{10}$$

$$\mathrm{Pr}_{film} = \frac{C_{pfilm}\mu_{film}}{\kappa_{film}} \qquad \text{(Prandtl number)} \tag{11}$$

where g represents the gravitational acceleration; the subscript *film* represents ambient properties evaluated at the film temperature [$T_{film} = (T_s + T_{amb})/2$]; T_s is the surface temperature, and ξ_{film} is the isobaric volumetric expansion coefficient. ξ_{film} is a thermodynamic property that can be obtained analytically from the equation of state. It is given by (Incropera and DeWitt, 1996)

$$\xi_{film} = -\frac{1}{\rho_{film}}\left(\frac{\partial \rho_{film}}{\partial T_{film}}\right)_P \tag{12}$$

For forced convection, the heat transfer correlation proposed by Churchill and Bernstein (1977) is used. This correlation given below is said to cover the entire range of Reynolds number for which data are available as well as a wide range of Prandtl numbers:

$$\frac{h_{for} D_{out}}{\kappa_{film}} = \left\{ 0.30 + \frac{0.62\ \mathrm{Re}_{film}^{1/2}\mathrm{Pr}_{film}^{1/3}}{[1 + (0.4/\mathrm{Pr}_{film})^{2/3}]^{1/4}} \times \left[1 + \left(\frac{\mathrm{Re}_{film}}{282{,}000}\right)^{5/8} \right]^{4/5} \right\} \tag{13}$$

Pressure and thermal stresses

Tangential (hoop) and axial stresses are the driving forces responsible for fracture propagation in the longitudinal and circumferential directions, respectively, with the latter leading to full bore rupture. Table 1 presents the corresponding equations for the pressure and thermal stresses.

Fracture propagation

As mentioned earlier, the quasi-adiabatic expansion of the escaping fluid will result in a cold-temperature front propagating away from the rupture plane. If this temperature falls below the pipeline material ductile to brittle transition, a significant drop in the material fracture toughness would occur (Parton, 1992). Depending on the prevailing thermal and pressure stresses in the defect plane, this transition could in turn lead to a secondary more catastrophic running brittle fracture, resulting in a massive release of the pressurized inventory.

For brittle materials, the critical facture toughness K_c, below which a fracture propagates, is given by (Irwin, 1957)

$$K_c = Y\sigma\sqrt{\pi a_l} \tag{14}$$

where σ is the sum of the pressure and thermal stresses. Y is a shape factor (see later discussion) depending on the crack length and geometry, with a_l representing the half crack length.

Table 1. Pipe Wall Tangential and Axial Thermal and Pressure Stress Equations*,**

	Thermal	Pressure
Tangential	$\frac{M_1}{r^2}\left[\frac{r^2+a^2}{b^2-a^2}\int_a^b Trdr+\int_a^r Trdr-Tr^2\right]$	$A_1\left(1+\frac{b^2}{r^2}\right)$
Axial	$M_1\left[\frac{2}{b^2-a^2}\int_a^b Trdr-T\right]$	A_1
	$M_1=\frac{\tau E}{1-\mu}\qquad A_1=\frac{P_i}{R^2-1}\qquad R=\frac{b}{a}$	

* From Popov (1999) and Timoshenko and Goodier (1987).
**τ, E, and μ are, respectively, the coefficient of thermal expansion, modulus of elasticity, and Poisson's ratio; T is pipe wall temperature; and P_i is internal pressure.

Results and Discussion

Case study

The following describes the results of the application of the above facture propagation model to a hypothetical puncture of a pressurized pipeline. Table 2 presents the prevailing conditions before its rupture, as used in the implementation of this model.

The pipe wall is assumed to be made of carbon steel with a ductile to brittle transition temperature (DBTT) of −15°C (Roberts, 1999). Values of the fracture toughness above and below the DBTT are taken as 95 and 40 MPa $m^{0.5}$, respectively (Roberts, 1999). These values are assumed to remain constant at any temperature away from the DBTT.

For the sake of an example, it is assumed that the initial defect is in the form of a 5 mm diameter circular puncture with a 0.05 m longitudinal hairline crack extending from its side as depicted below in Figure 6a. This type of failure geometry could result from an impact with a mechanical digger as an example. It is also typical of corrosion-induced defects. The isolated pipeline length is taken as 1 km, with the defect being formed at a distance of 250 m from the high-pressure end.

Two credible failure scenarios involving isolated and nonisolated releases are considered to investigate their effect on the defect stability. In the isolated case, it is assumed that pumping of the feed ceases 120 s after pipeline failure, whereas in the nonisolated case, pumping continues throughout the discharge process.

Figure 2 shows the variation of the radial temperature profiles (across the pipeline thickness) at the defect plane at different time intervals during the depressurization for the isolated failure scenario. A typical computational run time for this simulation and the subsequent data presented in the proceeding was about 2.5 h using a Pentium IV 2400 MHz computer.

Table 2. Pipeline Rupture Data*

Feed pressure (bara)	117
Feed temperature (°C)	20
Feed flow rate (kg/s)	34.5
Pipeline thickness (mm)	19
Pipeline nominal inner diameter (m)	0.419
Pipeline Density (kg/m^3)	7854
Pipeline thermal conductivity (W/mK)	53.6
Poission ratio	0.3
Coefficient of thermal expansion (K^{-1})	13×10^{-6}
Modulus of elasticity (MPa)	20.7×10^4
Wind velocity (m/s)	6.5

*Pipeline inventory (mol %): CH_4 (98.2), C_2H_6 (1.15), C_3H_8 (0.48), i-C_4H_{10} (0.11), N_2 (0.06).

For the conditions tested, the data indicate that the temperature variation across the pipe wall thickness is negligible. The maximum temperature drop is only 5 K after depressurization and, consequently, the associated thermal stresses in the radial direction may be safely ignored.

Figures 3 and 4 show the corresponding transient axial pipe temperature profiles at different time intervals in the proximity of the puncture plane for the isolated and nonisolated failure scenarios, respectively. The corresponding DBTT is also indicated for reference. In a referral to the isolated pipeline data (Figure 3), it is clear that the rapid expansion of the escaping inventory results in significant cooling of the pipe wall, with the effect becoming more pronounced with time and distance toward the puncture plane. The pipe wall temperature reaches the DBTT of 258 K, 30 s after puncture dropping to 240 K at 2700 s. Similar effects are observed in the case of nonisolated release (Figure 4). However, compared to the isolated release, the expansion-induced cold-temperature front moving away

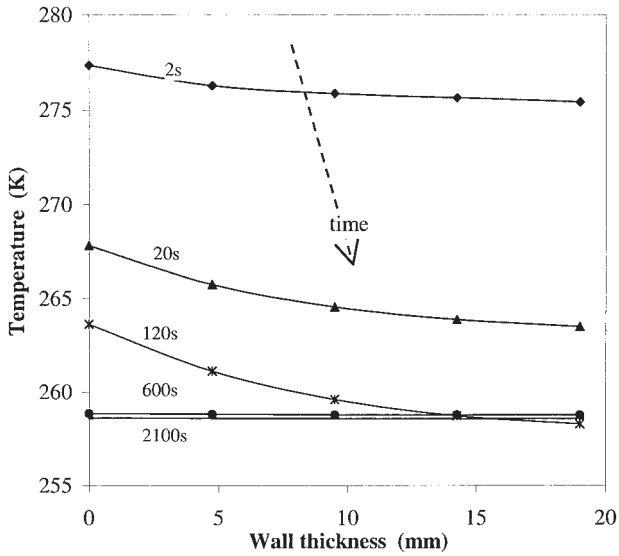

Figure 2. Transient variation of the radial temperature profile at the crack tip at different time intervals after depressurization for isolated release.

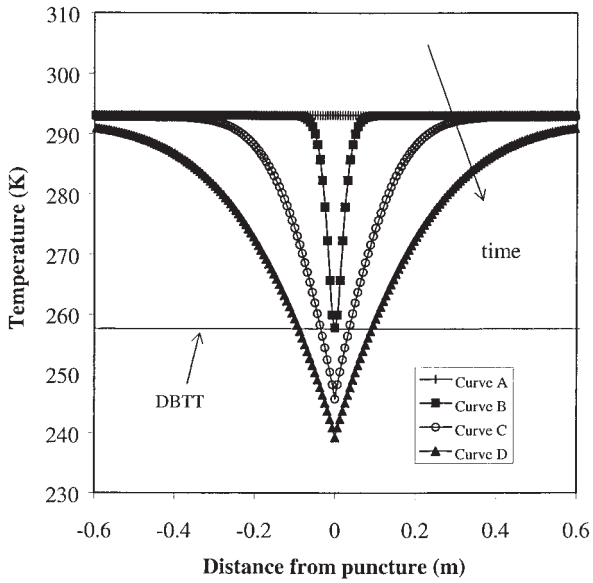

Figure 3. Transient variation of the axial temperature profiles in the vicinity of the defect plane for isolated discharge.

Curve A: 0 s; Curve B: 30 s; Curve C: 600 s; Curve D: 2700 s.

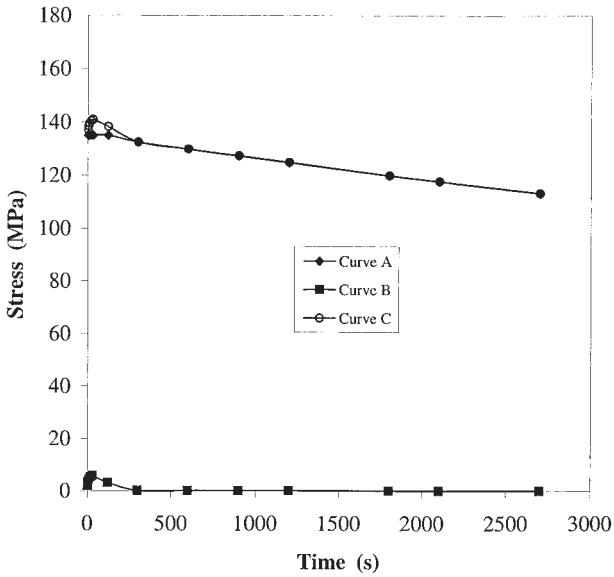

Figure 5. Variation of stress at crack tip with time during isolated discharge.

Curve A: Pressure stress; Curve B: thermal stress; Curve C: total stress.

from the rupture plane is confined to significantly smaller distances (0.2 m at 2700 s compared with 0.6 m at 2700 s). Also, the drop in the wall temperature is almost instantaneous.

Clearly, under such circumstances, it is imperative to ascertain whether the significant reduction in the pipe wall fracture toughness, coupled with the accompanying pressure and thermal stresses, may be sufficient to undermine the pipeline's mechanical integrity.

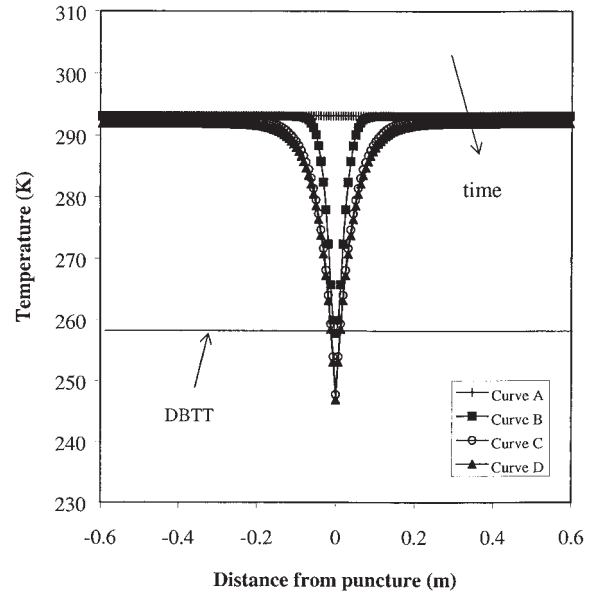

Figure 4. Transient variation of the axial temperature profiles in the vicinity of the defect plane for nonisolated discharge.

Curve A: 0 s; Curve B: 30 s; Curve C: 600 s; Curve D: 2700 s.

Figure 5 shows the transient variations of the prevailing pressure (hoop: curve A) and thermal (tangential: curve B) stresses at the crack tip during depressurization for the isolated pipeline. Curve C shows the corresponding total stresses. As may be observed, the thermal stresses are insignificant compared to the pressure stresses. However, it should be noted that the expansion-induced cooling of the pipeline plays a major role in weakening the pipeline mechanical integrity by reducing its fracture toughness and thus its resistance to withstanding the pressure stresses.

Figures 6a–6d provide a pictorial timeline simulation corresponding to four critical stages of crack growth for the isolated pipeline failure scenario. The corresponding calculation algorithm for determining the defect length that accounts for the pertinent thermodynamic, fluid dynamics, fracture mechanics, and heat transfer effects (as discussed in the theory section) is presented in Figure 7. The shape factors Y required for the calculation of the critical fracture toughness (Eq. 14) for each of the four stages of fracture propagation obtained from the literature are given in the same figure (Eqs. 15–21).

Stage 1: 0–30 s after Depressurization (Figure 6a). Crack growth commences when the temperature at any point at the defect/puncture boundary drops below the DBTT and $K_c > K_{mat}$. This occurs 30 s after depressurization and is marked by the onset of crack growth from the left-hand side of the puncture plane. It is noteworthy that at this early stage of depressurization, the preexisting fracture on the right-hand side of the puncture does not grow because the temperature at its tip (0.05 m from the puncture plane) has not yet reached the DBTT.

Stage 2: 30–1080 s after Depressurization (Figure 6b). Over the period from 30 to 1080 s after depressurization, a crack on the left of the puncture starts to grow. There is no crack growth on the right-hand side of the puncture because the temperature at the crack tip to the right is still above the DBTT.

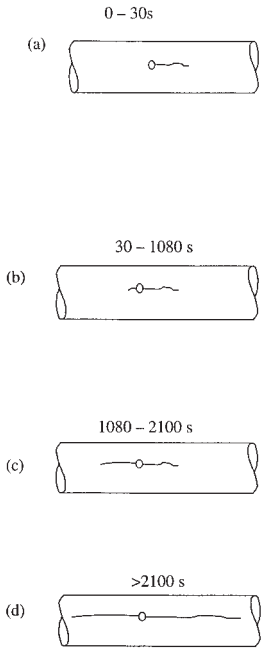

$$Y = \left[1 + 0.2(1-s) + 0.3(1-s)^6\right] Y_O \quad (15)$$

$$Y_o = 2.243 - 2.64s + 1.352s^2 - 0.248s^3 \quad (16)$$

$$s = \frac{a_i}{r_h + a_i} \text{ (Tada et al., 2000)} \quad (17)$$

$$Y(\lambda) = (1 + 1.25\lambda^2)^{0.5} \quad 0 \le \lambda \le 1 \quad (18)$$

$$Y(\lambda) = 0.6 + 0.9\lambda \quad 1 \le \lambda \le 5 \quad (19)$$

$$\lambda = ((a_i + a_j) + dh)/2 \,.[\, b(b-a)]^{0.5} \quad (20)$$

(Folias 1965; Erdogan and Kibbler, 1969)

$$Y = 1 + (1-s)\left[0.5 + 0.743(1-s^2)\right] \quad (21)$$

(Newman 1971; Tada et al., 2000)

Figure 6. Schematic representation of various critical stages of fracture growth at different time intervals during isolated release.

(a) and (b) are respectively the inner and outer pipe radius with a_i and a_j representing the respective crack lengths to the right and left of the defect. d_h and r_h are the puncture diameter and radius, respectively.

This stage of crack propagation ends when the crack lengths on either side of the puncture plane are equal.

Stage 3: 1080–2100 s after Depressurization (Figure 6c). The onset of stage 3 is marked by the crack length on the left side of the puncture becoming equal to the right side initial crack length (0.05 m). A further decrease in pressure results in both cracks propagating at the same rate.

Stage 4: Catastrophic Pipeline Rupture (>2100 s) (Figure 6d). At stage 4 the crack length is the maximum value sustainable by the pipe before becoming unstable. This leads to a running fracture and catastrophic pipeline failure.

Figure 8 shows the transient variation of defect length with time after puncture for the isolated release. The defect length is taken as the summation of the crack length and the puncture diameter. Curve A shows the actual defect length, whereas curve B shows the corresponding critical defect length required to cause catastrophic failure. Depressurization of the pipeline results in a significant and rapid increase in defect length. Catastrophic failure corresponding to the point of intersection for curves A and B occurs some 2100 s after puncture as indicated above.

Figure 9 shows the same data as in Figure 8 but for nonisolated release. Curve A indicates no crack growth for the first 30 s of discharge. This initial stability is explained by the fact that during the early depressurization period, the metal's temperature at the edge of the defect is higher than DBTT. However, subsequent to this period, the defect length increases by about 15 mm some 200 s after depressurization and remains stable. Additionally, because throughout the depressurization process the actual defect length remains well below the critical defect length (curve B), catastrophic pipeline failure during nonisolated discharge is highly unlikely.

Figure 10 shows the corresponding data for the variation of crack length with time for isolated release but assuming isothermal decompression. The data clearly demonstrate the importance of taking into account the expansion-induced cooling effects of the depressurizing medium. Ignoring such effects will lead to the erroneous conclusion of a stable defect.

Interestingly, the results of a similar analysis assuming an initial circumferential defect orientation fail to indicate crack propagation. This is explained by the fact that for a cylindrical geometry, the axial stress required for crack growth in the circumferential direction is double that for crack propagation in the longitudinal direction.

Conclusion

Although the study of low-temperature–induced brittle fracture in pressurized vessels after rapid depressurization or blowdown has received considerable attention, little work of a similar nature has been reported in the case of pressurized pipelines. This is despite the fact that significantly greater amounts of hydrocarbons are transported in long pipelines compared to those stored in pressurized vessels. In addition, a number of incidents in recent years have indicated running fracture as a common mode of pipeline failure.

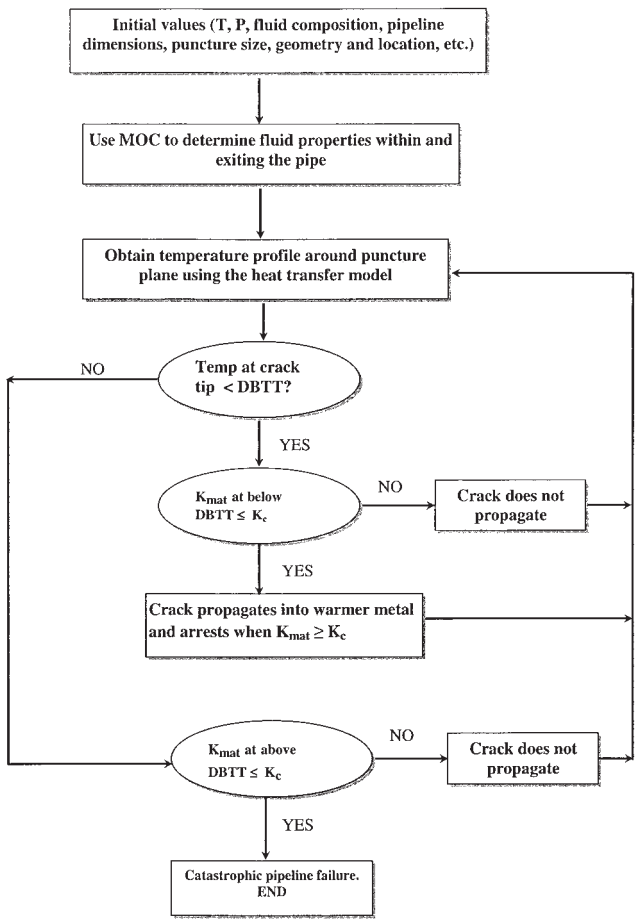

Figure 7. Fracture propagation calculation flow algorithm.

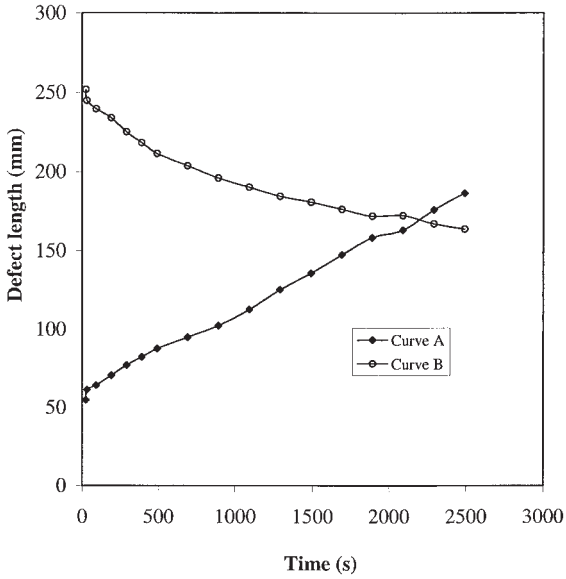

Figure 8. Variation of defect length with time for isolated discharge.

Curve A: Actual defect length; Curve B: defect length required to cause running fracture.

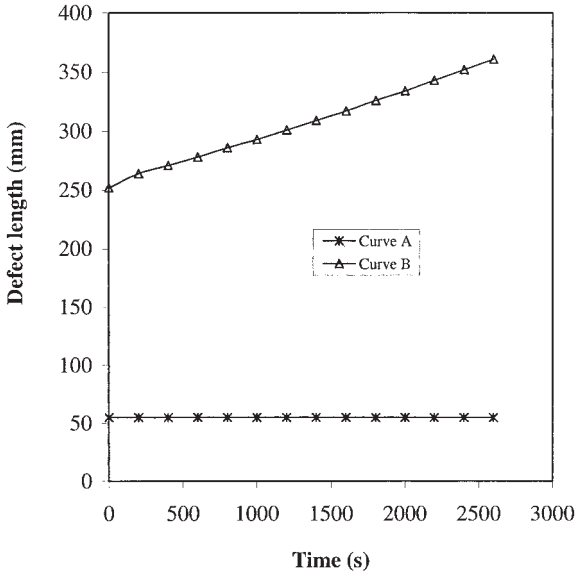

Figure 10. Variation of defect length with time for isolated discharge assuming isothermal release.

Curve A: Actual defect length; Curve B: defect length required to cause catastrophic failure.

This report provides a description of the development of a rigorous mathematical model for simulating low-temperature–induced brittle fracture of pressurized pipelines. The model accounts for all of the important processes taking place during depressurization, including real fluid behavior as well as the accompanying thermal and pressure stresses in the pipe wall.

A pictorial timeline presentation based on a hypothetical case example, starting with the puncture of an isolated pressurized pipeline containing a multicomponent hydrocarbon mixture, is used to elucidate the sequence of events leading to its catastrophic failure. The expansion-induced cooling of the escaping hydrocarbon results in a cold-temperature front moving away from the puncture plane, reaching temperatures well below the pipeline material's ductile to brittle transition temperature. This results in a significant decrease in the fracture toughness, thereby weakening the pipe wall.

The accompanying pressure stresses in the pipe wall, far exceeding the thermal stresses, are found to ultimately undermine the pipeline's mechanical integrity by transforming the initial defect into a running fracture.

Although a delay in isolation of the pipeline by maintaining the feed flow results in similar orders of magnitude drop in the pipe wall temperature and stresses compared to that in the isolated pipeline, such effects are found to be confined to close proximity of the defect plane. This has the effect of limiting the growth of the defect below the value necessary to initiate a running fracture. As such, catastrophic pipeline failures during normal flow are therefore unlikely.

The above finding presents an interesting dilemma as in practice whenever possible the puncture of the pipeline is universally followed by its immediate isolation using emergency shutdown valves. Although the above has the effect of limiting the amount of inventory escaping to the isolated pipeline section, it may well encourage low-temperature–induced effects, thus leading to brittle fracture of the pipeline.

The results of this study highlight the importance of accounting for low-temperature–induced brittle fracture as a potentially serious failure scenario when undertaking the safety assessment of pressurized pipelines. The model described herein can be used as an effective tool for mitigating such failures through better pipeline design, improved material selection, and appropriate emergency action.

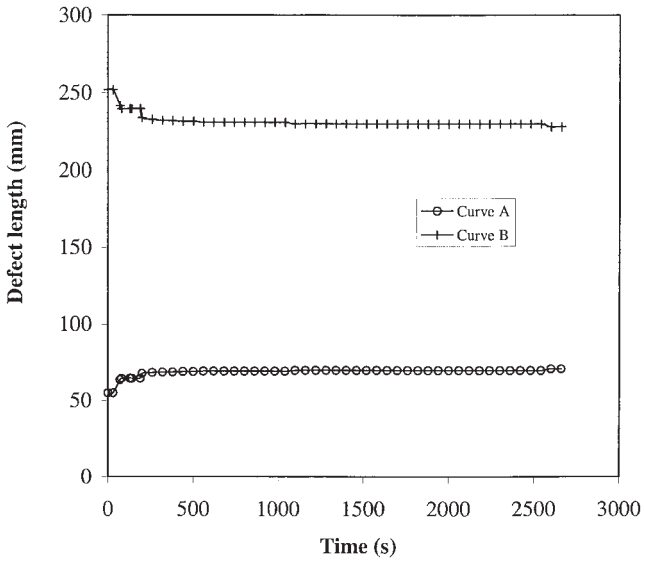

Figure 9. Variation of defect length with time for the nonisolated discharge.

Curve A: Actual defect length; Curve B: defect length required to cause running fracture.

Literature Cited

American Petroleum Institute (API), "Recommended Practice 579," *Fitness-for-Service*, 1st Edition, API, Washington, DC (2000).

Assael, M. J., J. P. Martin Trusler, and T. Tsolakis, *Thermophysical Properties of Fluids*, Imperial College Press, London (1996).
Barlas, S., "Pipeline Safety. Law Reauthorisation, " *Pipeline Gas J.*, **226**(4), 6 (1999).
Churchill, S. W., and M. Bernstein, "Correlating Equations for Forced Convection from Gases and Liquids to a Circular Cylinder in Cross-Flow," *J. Heat Transfer*, **99**, 300 (1975).
Churchill, S. W., and H. H. S. Chu, "Correlating Equations for Laminar and Turbulent Free Convection from a Horizontal Cylinder," *Int. J. Heat Mass Transfer*, **18**, 1049 (1975).
Cullen, W. D., *The Public Inquiry into the Piper Alpha Disaster*, Dept. of Energy, HMSO, London (1990).
de Reuck, K. M., R. J. B. Craven, and A. E. Elhassan, *Transport Properties of Fluids: Their Correlation, Prediction and Estimation,* J. Millat, J. H. Dymond, and C. A. Nieto de Castro, eds., IUPAC, Cambridge Univ. Press, Cambridge, UK (1996).
Duffy, A. R., "The Effect of Warm Prestressing on Fracture Toughness," Proc. of the 4th Symposium on Line Pipe Research, Paper H, pp. H10 and H11 (1969).
Environmental Defence, News Release, 3 Feb., New York (1999).
Erdogan, F., and Kibbler, J. J., "Cylindrical and Spherical Shells with Cracks," *Int. J. Fracture Mech.*, **5**, 229 (1969).
Folias, E. S., "An Axial Crack in a Pressurised Cylindrical Shell," *Int. J. Fracture Mech.*, **1**, 104 (1965).
Gnielinski, V., "New Equations for Heat and Mass Transfer in Turbulent Pipe and Channel Flows," *Int. Chem. Eng.*, **16**, 359 (1976).
Haque, M. A., S. M. Richardson, and G. Saville, "Blowdown of Pressure Vessels. I. Computer Model," *Trans IChemE Part B: Proc. Safety Environ. Protect.*, **70**(BI), 1 (1992).
Holman, J. P., *Heat Transfer*, McGraw-Hill, New York (1986).
Horsley, D. J., "Background to the Use of CTOA for Prediction of Dynamic Fracture Arrest in Pipelines," *Eng. Fracture Mech.*, **70**, 547 (2003).
Incropera, F. P., and D. P. DeWitt, *Fundamentals of Heat and Mass Transfer*, 4th Edition, Wiley, New York (1996).
Irwin, G. R., "Analysis of Stresses and Strains Near the End of a Crack Transversing a Plate," *Trans. ASME J. Appl. Math.*, **24**, 361 (1957).
Ives, K. D., A. K. Shoemaker, and R. F. McCartney, "Deformation during a Running Shear Fracture in Line Pipe," *ASME J. Eng. Mater. Technol.*, **96** (1974).
Mahgerefteh, H., P. Saha, and I. G. Economou, "A Study of the Dynamic Response of Emergency Shutdown Valves Following Full Bore Rupture of Gas Pipelines," *Trans. IChemE, Part B*, **75**, 201 (1997).
Mahgerefteh, H., P. Saha, and I. G. Economou, "Fast Numerical Simulation for Full Bore Rupture of Pressurized Pipelines," *AIChE J.*, **45**(6), 1191 (1999).
Mahgerefteh, H., P. Saha, and I. G. Economou, "Modelling Fluid Phase Transition Effects on Dynamic Behaviour of ESDV," *AIChE J.*, **46**(5), 997 (2000).
Mahgerefteh, H., and S. M. A. Wong, "A Numerical Blowdown Simulation Incorporating Cubic Equations of State," *Comput. Chem. Eng.*, **23**(9), 1309 (1999).
Markatos, N. C., and S. M. Rawnsley, "Simulation of a Small-Break Loss-of-Coolant Accident in a Pressurised Water Reactor," *Int. J. Model. Simul.*, **4**(2), 66 (1984).
Markatos, N. C., S. M. Rawnsley, and D. B. Splading, "Heat Transfer during a Small-Break Loss-of-Coolant Accident in a Pressurised Water Reactor: A Parametric Study for a 4-in. Lower-Plenum Break," *Int. J. Heat Mass Transfer*, **27**(8), 1379 (1984).
Massey, B. S., *Mechanics of Fluids*, Van Nostrand Reinhold, Wokingham, UK (1983).
Maxey, W. A., "Fracture Initiation, Propagation and Arrests," Proc. of Fifth Symposium on Line Pipe Research, American Gas Association, Washington, DC (1974).
Maxey, W. A., J. F. Kiefner, and R. J. Eiber, "Ductile Fracture Propagation Resistance of Rising Shelf Controlled Steels," Proc. of ASM Symposium on What Does Charpy Energy Really Mean? (1975).
Michelsen, M. L., "The Isothermal Flash Problem. Part I. Stability," *Fluid Phase Equilib.*, **9**, 1 (1982a).
Michelsen, M. L., "The Isothermal Flash Problem. Part II. Phase-Split Calculation," *Fluid Phase Equilib.*, **9**, 21 (1982b).
Michelsen, M. L., "Multi-phase Isenthalpic and Isentropic Flash Algorithms," *Fluid Phase Equilib.*, **33**, 13 (1987).
Newman, J. C., "An Improved Method of Collocation for the Stress Analysis of Cracked Plates with Various Shape Boundaries," NASA Technical Note, NASA TN D-6376 (1971).
Oke, A., H. Mahgerefteh, I. Economou, and Y. Rykov, "A Transient Outflow Model for Pipeline Puncture," *Chem. Eng. Sci.*, **58**, 4591 (2003).
Ozisik, M. N., *Heat Conduction*, Wiley, New York (1980).
Parton, P. V., *Fracture Mechanics From Theory to Practice*, Gordon & Breach Science, New York (1992).
Peng, D. Y., and D. B. Robinson, "A New Two-Constant Equation of State," *Ind. Eng. Chem. Fundam.*, **15**, 59 (1976).
Philbin, M. T., "The Simulation of Transient Phenomena in Multiphase Production Systems," United Kingdom Atomic Energy Authority (UKAEA) Harwell Report AEA-APS-0177 (1991).
Picard, D. J., and P. R. Bishnoi, "Calculation of the Thermodynamic Sound Velocity in Two-Phase Multi-Component Fluids," *Int. J. Multiphase Flow*, **13**(3), 295 (1987).
Picard, D. J., and P. R. Bishnoi, "The Importance of Real-Fluid Behaviour and Non-Isentropic Effects in Modelling Compression Characteristics of Pipeline Fluids for Application in Ductile Fracture Propagation Analysis," *Can. J. Chem. Eng.*, **66**, 3 (1988).
Popov, E. P., *Engineering Mechanics of Solids*, Prentice Hall, Englewood Cliffs, NJ (1999).
Richardson, S. M., and G. Saville, "Blowdown of Pipelines," *Society of Petroleum Engineers Europe 91*, Paper SPE 23070, Aberdeen, UK, p. 369 (1991).
Rinebolt, J. A., and W. J. Harris, "Effect of Alloying Elements on Notch Toughness of Pearlitic Steels," *Trans. Am. Soc. Metals*, **43** (1951).
Roberts, S. G., "Multiscale Phenomena in Plasticity: From Experiments to Phenomenology," Proc. of Modelling and Materials Engineering, Sep. 8–19 1999, Ouranopolis, Greece (1999).
Rohsenow, W. M., J. P. Hartnett, and Y. I. Cho, eds., *Handbook of Heat Transfer*, 3rd Edition, McGraw-Hill, New York (1988).
Saha, P., "Modelling the Dynamic Response of Emergency Shutdown Valves Following Full Bore Rupture of Long Pipelines," PhD Thesis, University College London, UK (1997).
Saville, G., S. M. Richardson, and P. Barker, "Leakage in Ethylene Pipelines," *Trans. IChemE.*, **82B**, 61 (2004).
Steiner, D., and J. Taborek, "Flow Boiling Heat Transfer in Vertical Tubes Correlated by an Asymptotic Method," *Heat Transfer Eng.*, **13**(2), 43 (1992).
Tada, H., P. Paris, and G. Irwin, *The Stress Analysis of Cracks Handbook*, 3rd Edition, American Society of Mechanical Engineers, New York (2000).
Techo, R., R. R. Tickner, and R. E. James, "An Accurate Equation for the Computation of the Friction Factor for Smooth Pipes from the Reynolds Number," *J. Appl. Mech.*, **32**, 443 (1965).
Timoshenko, S. P., and J. N. Goodier, *Theory of Elasticity*, McGraw-Hill, New York (1987).
Zucrow, M. J., and J. D. Hoffman, *Gas Dynamics*, Vols. I and II, Wiley, New York, p. 297 (1976).

Manuscript received Feb. 23, 2005, and revision received Sept. 20, 2005.